Bulletin of the Seismological Society of America, Vol. 102, No. 1, pp. 352–360, February 2012, doi: 10.1785/0120110096

Ⓔ

Scaling Relationships of Source Parameters for Slow Slip Events

by Haiying Gao,* David A. Schmidt, and Ray J. Weldon II

Abstract To better understand the physical mechanisms of slow slip events (SSEs) detected worldwide, we explore the scaling relationships of various source parameters and compare them with similar scaling laws for earthquakes. These scaling relationships highlight differences and similarities between slow slip events and earthquakes and hold implications for the degree of heterogeneity and fault-healing characteristics. The static stress drop remains constant for different-sized events as is observed for earthquakes. However, the static stress drop of slow slip events is within a range of 0.01–1.0 MPa, 1–2 orders of magnitude lower than that found for earthquakes, which could be related to the low stress state on the fault. The average rupture velocity, ranging from kilometers per second to kilometers per day, decreases linearly with increasing seismic moment in log–log space, unlike earthquakes that are nearly constant. This inverse relationship of rupture velocity with seismic moment could be related to the heterogeneity of fault properties. Slow slip events typically have ratios of event duration over dislocation rise time less than 3, while earthquakes have ratios greater than 3. This indicates that slow slip events are less pulselike than earthquakes in their mode of propagation and suggests that the healing behind the rupture front is delayed. The recurrence statistics of slow slip events on the northern Cascadia subduction zone are weakly time predictable and moderately antislip predictable (that is, the event size and preevent recurrence interval are anticorrelated), which may indicate that healing between events strengthens the fault with time.

Online Material: Table of source parameters and data sources.

Introduction

In the last decade, a new mode of faulting, referred to as slow slip events (SSEs), has been detected on many of the world's subduction zones. Slow slip events, which represent the transient release of strain over the duration of days to weeks, occur downdip of the transition zone between the locked seismogenic zone and the free-slipping zone on the plate interface, and fluids are thought to be critical for its occurrence (e.g., Obara, 2002; Rogers and Dragert, 2003). Slow earthquakes have also been reported in other tectonic environments such as the San Andreas fault (Linde *et al.*, 1996) and Hawaii (Segall *et al.*, 2006; Montgomery-Brown *et al.*, 2009). Although several hypotheses have been proposed to explain these events (e.g., Ito *et al.*, 2007; Schwartz and Rokosky, 2007; Brodsky and Mori, 2007; Ide, 2008; Liu and Rice, 2009; Ando *et al.*, 2010; Hawthorne and Rubin, 2010; Ide, 2010; Liu and Rubin, 2010; Peng and Gomberg, 2010; Shibazaki *et al.*, 2010), the physical mechanisms are still not fully understood.

A source parameter scaling law is an empirical relationship between source parameters (e.g., fault dimensions, seismic energy, and stress drop) that is not explicitly predicted by theory. The empirical scaling relationships of earthquake source parameters provide important insights and constraints on the dynamics of earthquake rupture. The scaling of source parameters has established several widely accepted characteristics of the faulting process, such as the independence of static stress drop on earthquake size (Kanamori and Anderson, 1975) and the propagation of rupture in a pulselike manner (Heaton, 1990) with a nearly constant rupture velocity (Geller, 1976).

Ide *et al.* (2007) was the first work to explore the source scaling of SSEs. They proposed a general logarithmic scaling law of seismic moment M_0 and event duration T for SSEs where $M_0 \sim T$, which is different than the $M_0 \sim T^3$ relationship observed for earthquakes (Furumoto and Nakanihshi, 1983; Houston, 2001). This implies that to release a similar amount of energy, SSEs need a much longer rupture duration than earthquakes. This difference in the scaling prompted Ide *et al.* (2007) to describe slow slip, tremor, and low-frequency earthquakes as representing a unique physical process distinct from that of earthquakes. Schwartz and Rokosky (2007) also noted the distinct moment-duration

*Now at the Seismology Laboratory, University of Rhode Island.

relationship of SSEs. Peng and Gomberg (2010) found that SSEs follow the same general trend, but other aseismic slip processes (including afterslip, earthquake swarms, and landslides) fill out a broader continuum in the moment-duration parameter space. Meade and Loveless (2009) considered the scaling law for the average particle velocity versus moment. Obara (2010) explored the relationship of moment versus fault area for tremors and inferred a static stress drop less than 0.1 MPa. Finally, Brodsky and Mori (2007) examined the relationship between fault slip, rupture length, and duration for creep events versus earthquakes. They suggested that significant strength heterogeneity and dynamic overshoot for seismogenic faults may explain the higher stress drops for earthquakes when compared to aseismic slip events.

In this work, we expand on the scaling behavior of SSEs in order to provide important insights about the faulting processes. Taking advantage of the variety and the increasing amount of SSEs detected on subduction zones, our major goal of this study is to evaluate the scaling relationships between several sets of source parameters including seismic moment versus rupture area, event duration, average rupture velocity, and recurrence interval, respectively. We also explore the relationship of fault length versus fault width and event duration versus rise time. These source parameter comparisons define the general relationships applicable to most SSEs and help us better constrain the rupture dynamics of this phenomenon, while also providing basic constraints for numerical models. Meanwhile, our findings help to illustrate the similarities and differences between earthquakes and SSEs. Our study characterizes the pulselike statistics of SSEs and tests the recurrence behavior of events in Cascadia.

Slow Slip Data Set

We compile source parameters of worldwide SSEs to explore the scaling relationships of this phenomenon, including seismic moment M_0, static stress drop $\Delta\sigma$, average fault slip $\bar{D}$, average rupture velocity $\bar{V}_{\mathrm{rpt}}$, fault dimension (rupture area A, along-strike fault length L, and downdip width W), event duration T, and dislocation rise time τ. There are two sources for the dataset used in this study: source parameters inferred directly from the slip distributions of Schmidt and Gao (2010) for the Cascadia subduction zone and source parameters reported in the literature for other subduction zones (e.g., Obara *et al.*, 2004; Brown *et al.*, 2005; Douglas *et al.*, 2005; Hirose and Obara, 2005; Wallace and Beavan, 2006; Ito and Obara, 2006; Hirose and Obara, 2006; Correa-Mora *et al.*, 2008, 2009; Hirose and Obara, 2010; Sekine *et al.*, 2010; see references in Ⓔ Table S1, available in the electronic supplement to this paper). Additionally, we also include documented aseismic slip on the San Andreas fault (Linde *et al.*, 1996) and Hawaii's south rift zone (Segall *et al.*, 2006; Montgomery-Brown *et al.*, 2009). In this study, we attempt to focus on a specific type of slow slip phenomenon in order to ensure that we are studying a consistent underlying process. Therefore, we exclude observations of aseismic slip from processes such as afterslip, landslides, glaciers, and earthquake swarms as explored by Peng and Gomberg (2010). All the data and references used in our analysis are listed in Ⓔ Table S1 (available in the electronic supplement to this paper).

For the Cascadia subduction zone, we use the catalog of SSEs solved by Schmidt and Gao (2010), which we briefly describe here. Using the extended network inversion filter, Schmidt and Gao (2010) inverted the daily GPS time series and resolved the time-dependent slip distributions of the 16 largest SSEs on the Cascadia subduction zone from 1998 to 2008. We update this catalog to include two 2009 events in April and August that we solve using the same methodology. We strive to extract source parameters from the slip distributions in a systematic way while also avoiding inversion artifacts. In our analysis, we only consider fault elements where the estimated slip is greater than 0.5 cm (which is considered to be the resolution of the inversion) on three or more adjoining fault elements within the depth range of 20–50 km. The average slip $\bar{D}$ of each event (~2–5 cm per event) is the average of the total slip accumulated on fault elements that match the criteria previously stated. The rupture length L, which ranges from 100 to 1000 kilometers, is the along-strike length following the 35-km slab depth contour. Similarly, the rupture area A is the cumulative area for all fault patches that satisfy the criteria. The total event duration T for each SSE is inferred from the starting and end dates of all GPS stations that record the transient signal in conjunction with the tremor activity. From this we infer the average rupture velocity by dividing the rupture length by the event duration, $\bar{V}_{\mathrm{rpt}} = L/T$. For SSEs propagating bilaterally along strike, the average rupture velocity is inferred as the average of the rupture velocities along each direction. The seismic moment is equal to $M_0 = \mu\bar{D}A$ with the rigidity $\mu = 40$ GPa.

The source parameters of these SSEs solved on the Cascadia subduction zone focus in a narrow range of moment magnitudes ($M_{\mathrm{w}} \sim 6.2$–6.7) with similar event durations (~2–7 weeks), which makes it difficult to explore the general logarithmic scaling relationships of SSEs. To better address this issue, we collect published source parameters for SSEs documented at other locations. For SSEs without published rupture velocity, we estimate the average rupture velocity by dividing the inferred fault length by the duration. The duration of these SSEs varies from seconds up to years, and the rupture velocity from kilometers per day to kilometers per second. This provides a larger dynamic range to study this phenomenon, especially by including tremor sequences detected in Japan that exhibit short durations and small seismic moments but fast propagation velocities. Source parameters published for earthquakes are also collected and used as a comparison with SSEs (Kanamori and Anderson, 1975; Geller, 1976; Heaton, 1990; Wald and Heaton, 1994; Wald *et al.*, 1996; Kanamori *et al.*, 1998; Yagi and Kikuchi, 2000; Hernandez *et al.*, 2001; Hwang *et al.*, 2001; Hanks and Bakun, 2002; Baumont *et al.*, 2002; Ji *et al.*, 2002; Yagi, 2004; Ishii *et al.*, 2005; Hanks and Bakun, 2008).

In this study, we are primarily interested in the general log–log trends between different source parameters. The scatter in the data along these trends is reflective of variations in inversion methodologies, source complexities (fault geometry, rupture history, etc.), and observational uncertainties. Comparing the scaling relationships of slow slip events in Cascadia with those from other subduction zones, the source parameters for Cascadia SSEs are more consistent and well constrained. Part of the reason is that these SSEs are from the same subduction zone and are determined with a consistent methodology. Source parameters inferred from the literature are estimated with a variety of inversion methodologies by different groups, making the data more scattered. This argues for the need to develop a consistent catalog of SSEs for numerical simulations and theoretical models to be tested against. Considering the variety and complexity of the data origins used in this study, we prefer to qualify the parameter uncertainties without providing quantitative standard errors. Most GPS studies can resolve fault slip on the order of ~1 cm, have temporal resolution on the order of days, and resolve rupture length on the order of tens-of-kilometers. The uncertainties on event duration and rise time would be similar to the temporal resolution. Thus, the uncertainty in the average rupture velocity would be ~25% of the velocity (~1.5 km/day in Cascadia) based on the propagation of errors. For fault area, the uncertainty would correspond to ~2.5 orders of magnitude, while the data range over 5+ orders of magnitude. The uncertainty of seismic moment and static stress drop would be less than an order of magnitude and ~25%, respectively. Finally, some regions of the parameter space are beyond the observational capabilities of the instrumentation. For example, the GPS network in Cascadia cannot fully resolve SSEs with moment magnitudes below ~6.

Empirical Scaling Laws of SSEs

We present and discuss each scaling law in the following subsections. In summary, the scaling laws suggest that both the aspect ratio (L/W, Fig. 1) and the static stress drop for SSEs are nearly constant (Fig. 2), as found for earthquakes. However, SSEs display a different dependence of event duration and average rupture velocity with seismic moment (Figs. 3, 4), and a much smaller ratio of event duration to dislocation rise time (Fig. 5). The recurrence statistics of the northern Cascadia events show that the seismic moment is anticorrelated to the preevent recurrence interval (Fig. 6).

Fault Length versus Width

The aspect ratio of earthquakes is found to be empirically constant, $L \sim 2W$, on average (Kanamori and Anderson, 1975; Geller, 1976). This relationship has been used historically to convert between width, length, and area of the fault surface, especially in cases where the direct observation of fault dimension is limited. The data for both SSEs and earthquakes fall within a range of aspect ratios from 1 to 4 (Fig. 1).

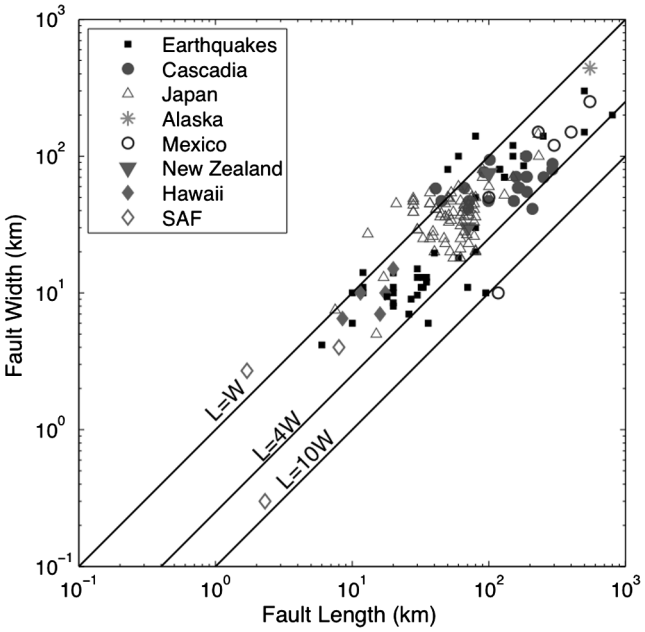

Figure 1. The relationship of along-strike fault length L versus downdip fault width W, for slow slip events (SSEs) on subduction zones, on Hawaii's south rift zone and on the San Andreas fault (SAF). Solid lines denote contours of constant aspect ratio. On average, the along-strike fault length is two times the downdip width for both slow slip events and earthquakes. The widths of SSE generation zone may be limited or saturated in the dip direction. The color version of this figure is available only in the electronic edition.

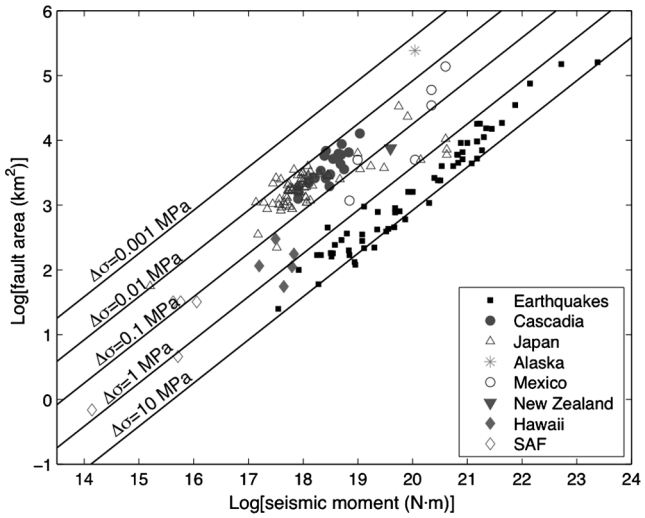

Figure 2. The logarithmic relationship of seismic moment M_0 versus fault area A, for slow slip events on subduction zones, on Hawaii's south rift zone and on the San Andreas fault (SAF). Solid lines mark constant static stress drop $\Delta\sigma$ calculated for a rectangular fault crack ($L \sim 2W$) for reference. Although there is scatter in the data, the static stress drop of slow slip events is nearly constant (0.01–1.0 MPa), 1–2 orders of magnitude lower than earthquakes (1–10 MPa). The color version of this figure is available only in the electronic edition.

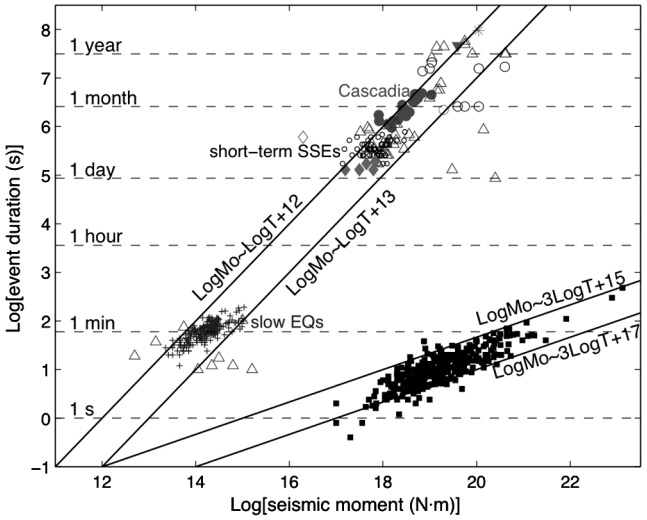

Figure 3. The relationship of seismic moment M_0 with event duration T for slow slip events in comparison to earthquakes (EQ). The horizontal dashed lines indicate contours of constant event duration. The Cascadia SSEs, a slow earthquake sequence (plus symbol, from Ide *et al.*, 2008), and short-term SSEs (small open circles, from Sekine *et al.*, 2010) all fall within the $\mathrm{Log}M_o \sim \mathrm{Log}T$ trend. Other markers are the same as Figures 1–2. The color version of this figure is available only in the electronic edition.

For the Cascadia events, the trend is nearly flat such that the fault width is roughly constant, whereas the length extends out to ~4 times the width of the largest events. This reflects the fact that the largest events are constrained within the downdip direction, but are allowed to propagate along strike. Therefore, the downdip source dimension may saturate for a particular geographic locality depending on the fault dip and thermal state of the downgoing slab (e.g., Ide, 2010). Nevertheless, the aspect ratio of about 2 best describes the entire catalog of SSEs over a broad range of fault lengths. We use this scaling to derive the theoretical relationship of seismic moment versus fault area, as discussed in the next section.

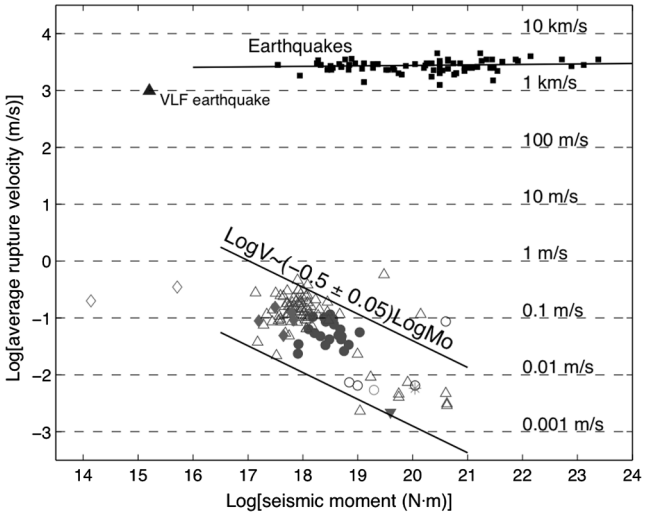

Figure 4. The inverse relationship of average rupture velocity with seismic moment for slow slip events. Markers are the same as in Figures 1–2. Earthquakes have a nearly constant rupture velocity whereas slow slip events show a decreasing rupture velocity with increasing seismic moment. Only one very low-frequency earthquake (solid triangle) is available (Ito and Obara, 2006). The solid lines denote the linear fit for short- and long-term slow slip events with durations longer than days without including the Hawaii and San Andreas fault data points. The color version of this figure is available only in the electronic edition.

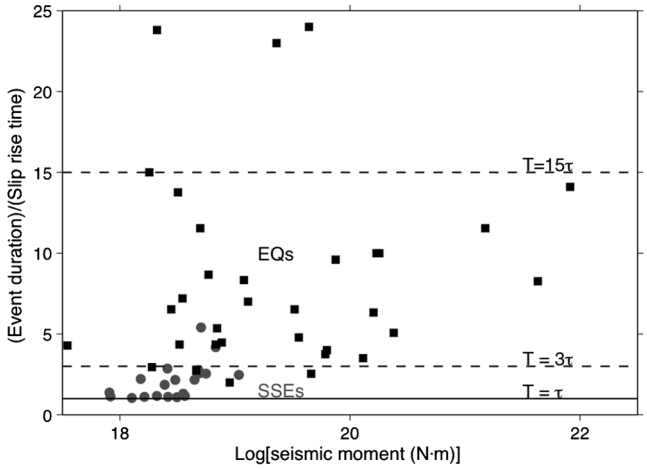

Figure 5. The ratio of event duration T to rise time τ as a function of seismic moment. The ratio T/τ is expected to be 1 for an expanding crack (solid horizontal line), whereas rupture pulses have large ratios since the total duration of the event far exceeds the time for slip to accumulate at a point on the fault. The ratio of event duration to rise time is smaller for slow slip events (SSEs, solid dots, less than 3) compared to earthquakes (solid squares, greater than 3). This indicates that slow slip events are less pulselike compared to earthquakes. The color version of this figure is available only in the electronic edition.

Seismic Moment versus Fault Area

The relationship of seismic moment M_0 and fault area A was explored for earthquakes by Kanamori and Anderson (1975) in which $\mathrm{Log}M_0$ scales with $(3/2)\mathrm{Log}A$. This relationship assumes that the aspect ratio of a rupture patch is independent of magnitude, which we find holds true for SSEs as well as earthquakes (Fig. 1). By combining the assumption of constant aspect ratio and the theoretical description of the stress drop on a crack, the following relationship was derived by Kanamori and Anderson (1975),

$$\mathrm{Log}M_0 = (3/2)\mathrm{Log}A + \mathrm{Log}\Delta\sigma + \mathrm{Log}C, \qquad (1)$$

where C is a nondimensional factor for the fault shape. When plotted on a graph for moment and area (fig. 2 in Kanamori and Anderson, 1975), the data were found to follow contours of constant stress drop within the range of 1–10 MPa, and this result established the constant stress drop model for large earthquakes.

Using data available for SSEs, we plot the log–log relationship of seismic moment to rupture area, which is found to be parallel to that of earthquakes (Fig. 2). By assuming the constant aspect ratio with equation (1), Figure 2 implies that

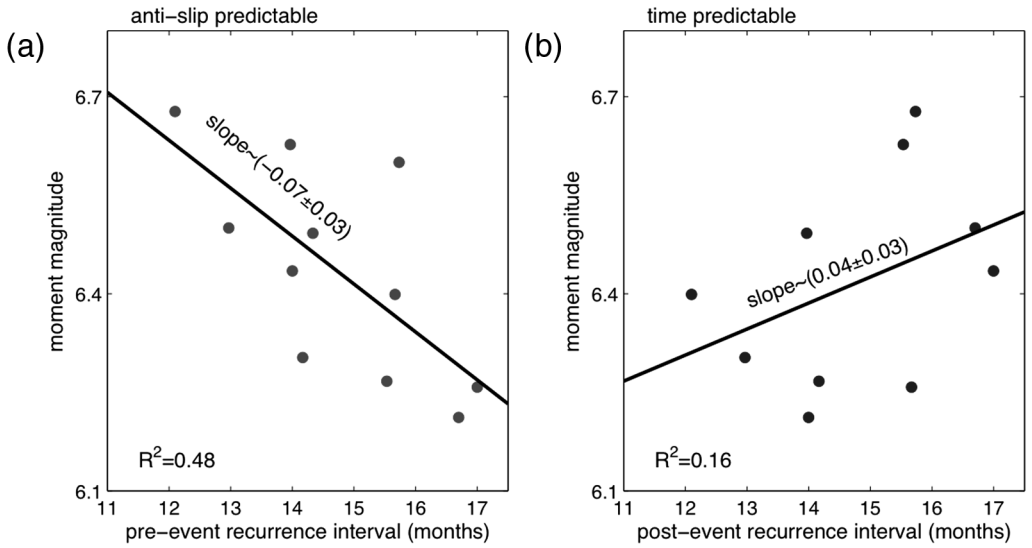

Figure 6. Recurrence statistics for slow slip events in northern Cascadia. (a) The slip predictable model requires that larger events are preceded by longer intervals. However, the data suggests that these parameters are moderately anticorrelated. (b) The time predictable model predicts larger events to be followed by longer intervals. These parameters appear to be weakly positively correlated. The color version of this figure is available only in the electronic edition.

the static stress drop for SSEs is also independent of event size and rupture area. Given a rectangular fault with $L = 2W$, the stress drop of SSEs is within a range of 0.01–1.0 MPa, generally 1–2 orders of magnitude smaller than earthquakes. Some of the scatter in Figure 2 likely relates to uncertainty in the actual geometry of the source rupture. One possible explanation for the low stress drop would be that the effective stress is very low on the fault. Seismic observations on subduction zones where SSEs occur suggest that the pore fluid pressure is near-lithostatic (Shelly *et al.*, 2006; Audet *et al.*, 2009), resulting in a very low effective normal stress. The low estimate of the effective normal stress limits the level of shear stress on the fault, which might be on the order of tens of kilopascals (e.g., Rubinstein *et al.*, 2007; Nadeau and Guilhem, 2009). Thus, the stress drop during an event would be limited to a fraction of the shear stress.

Within the groups of SSEs, events on the San Andreas fault and Hawaii appear to have higher stress drops (~0.1–1.0 MPa) than those on subduction zones (Fig. 2). The scatter in the data and the small sample size make a robust assessment difficult. The subduction setting provides ample sources of fluid that may result in or allow for relatively high pore pressure when compared with the transform setting of the San Andreas and hotspot environment of Hawaii. Abundant fluids may facilitate low effective stress and conditionally stable behavior on subduction zones. The lack of tremor associated with shallow aseismic slip in Hawaii (Montgomery-Brown *et al.*, 2009) and the San Andreas fault (Zhang *et al.*, 2010) may indicate that pore pressures are not as high in these regions as on those subduction zones where nonvolcanic tremor and SSEs are colocated (Rogers and Dragert, 2003; Obara *et al.*, 2004). In addition to their different tectonic environments, the depths at which the events occur are strikingly different, which may be a factor. Slow slip events on the San Andreas and in Hawaii occur at depths less than 10 km, while those on subduction zones occur at depths greater than 30 km. The lower temperature and pressure at these shallow depths allow for aseismic fault slip on velocity-strengthening fault zones without the need for high pore fluid pressures (Marone *et al.*, 1991).

Seismic Moment versus Event Duration

Ide *et al.* (2007) defined a linear scaling relationship of seismic moment versus event duration for slow earthquakes as $\mathrm{Log}M_0 \sim \mathrm{Log}T$. To explain this scaling, two models were proposed by Ide *et al.* (2007): the constant stress drop model and the constant slip model. Our present study strongly supports the constant stress drop model (Fig. 2). Here we reassess this logarithmic scaling relationship by adding data of more recent SSEs (Fig. 3), including two slow earthquake sequences in Japan (data from Ide *et al.*, 2008 and Sekine *et al.*, 2010). Note that there is a lack of observations in our dataset for seismic moment within ~1.0e15 – 1.0e17 N·m corresponding to duration ranging from minutes to days. A similar analysis was performed by Schwartz and Rokosky (2007) and Peng and Gomberg (2010), where the latter consider a broader class of aseismic phenomenon. The Cascadia SSEs, a slow earthquake sequence (Ide *et al.*, 2008), and short-term SSEs (Sekine *et al.*, 2010) all fall within the $\mathrm{Log}M_0 \sim \mathrm{Log}T$ trend. As pointed out by Ide *et al.* (2008), the lower slope characteristic of data from a particular study or geographic region may represent an artifact, potentially reflecting the saturation of a fault parameter from limited observations or the methodology.

Average Rupture Velocity versus Seismic Moment

By assuming $\mathrm{Log}M_0 \sim n\mathrm{Log}T$ (where n is the exponent) and constant static stress drop, one can infer the following general relationship,

$$-(3-n)/(3n)\mathrm{Log}M_0 = \mathrm{Log}\bar{V}_{\mathrm{rpt}} + \text{constant}. \quad (2)$$

Equation (2) indicates that if n is less than 3, the average rupture velocity $\bar{V}_{\mathrm{rpt}}$ decreases with the seismic moment, whereas if n is equal to 3, $\bar{V}_{\mathrm{rpt}}$ is independent of event size. For earthquakes, as shown by the empirical relation of seismic moment and event duration (Fig. 3), n is found to be ~3, supporting the independence of rupture velocity on seismic moment. For SSEs, n is approximately 1 as proposed (Ide *et al.*, 2007), predicting a decrease in rupture velocity with an increase in event size.

Here we explore the scaling of the rupture velocity for SSEs. The rupture characteristics for SSEs and nonvolcanic tremor often exhibit complex propagation behavior, including propagation reversals to the major trend along strike, updip migration faster than the along-strike propagation, and fast-then-slow rupture pattern along strike (Shelly *et al.*, 2007; McCausland *et al.*, 2010; Obara, 2010; Houston *et al.*, 2011). In this study, we only consider the average rupture velocity, which is calculated by dividing the rupture length by the event duration. Determining the rupture velocity from tremor is more problematic. Most studies report the propagation of tremor streaks (Shelly *et al.*, 2007; Obara, 2010), whereas few studies have resolved the rupture velocity of an individual event (Ito and Obara, 2006). Because of the difficulty in estimating the fault dimension and individual event duration from tremor, we focus on short- and long-term slow earthquakes (with durations longer than days, Fig. 4).

Based on the kinematic inversions of coseismic events from strong motion records, the rupture velocity of earthquakes is nearly constant (Geller, 1976). However, the rupture velocity of SSEs decreases with increasing seismic moment (Fig. 4) that follows the relationship $\mathrm{Log}\bar{V}_{\mathrm{rpt}} \sim (-0.5 \pm 0.05)\mathrm{Log}M_0$. The data suggest a coefficient of $n = 1.2 \pm 0.1$ for equation (2), which agrees well with $n = 1$ (Ide *et al.*, 2007). The rupture velocity of slow earthquakes varies from tens-of-kilometers per day to hundreds-of-meters per day with the seismic moment ranging from 10^{14}–10^{21} N·m, while being around kilometers per second for very low-frequency earthquakes (solid triangle in Fig. 4). The one data point for very low-frequency earthquakes supports the concept that smaller events rupture faster.

Initial attempts to model slow slip events with numerical simulations did not reproduce the dependence of velocity on moment that is suggested by Figure 4 (Liu and Rice, 2009; Shibazaki *et al.*, 2010). However, these early models assumed a planar fault with smoothly varying fault properties. More recent models have explored alternative formulations that produce a greater diversity of slip behaviors (Ariyoshi *et al.*, 2009; Ide, 2010; Ando *et al.*, 2010; Nakata *et al.*, 2011; Rubin, 2011). Drawing upon these numerical studies on SSEs and the traditional concept of an asperity model proposed for earthquakes (e.g., Aki, 1979; Johnson and Nadeau, 2002), we hypothesize that the dependence of velocity on magnitude could be related to the heterogeneity of fault properties on the SSE generation zone, such as the heterogeneous distribution of the pore fluid pressure, stress state, or friction. Faults that exhibit slow slip and tremor could consist of many small-sized stronger asperities surrounded by weaker regions. The asperity model for earthquakes was first extended to SSEs as a way to explain the variety of SSEs observed on subduction zones (Ito *et al.*, 2007).

It is proposed for earthquakes (Day, 1982) that the slip rise time is approximately $W_{\mathrm{eff}}/(2\bar{V}_{\mathrm{rpt}})$ for a long narrow fault where W_{eff} is the effective width of asperities. If we apply this relationship to nonvolcanic tremors using the extrapolated rupture velocity and rise time, the effective asperity width is on the order of hundreds-of-meters. Alternatively, slow slip exhibits a longer rise time and slower velocity that translates into an effective asperity size of a few tens-of-kilometers. Thus, tremor may initiate and propagate along small asperities at relatively fast velocities, while large-dimension slow slip propagates along the fault surface between the asperities at a slower velocity. This interpretation of the rupture dimensions is consistent with the model of Ando *et al.* (2010), in which the slow slip event covers the entire brittle-ductile transition zone and works as a trigger for low-frequency tremor on those small patches.

Rupture Duration versus Rise Time

The dislocation rise time of earthquakes is typically only 10%–20% of the event duration based on near-source observations (e.g., Beroza and Spudich, 1988; Heaton, 1990). Two classical models have been proposed to explain the short rise time: the self-healing pulselike rupture behavior (e.g., Heaton, 1990; Beeler and Tullis, 1996) and rupture propagation along a heterogeneous fault (e.g., Boatwright, 1988; Beroza and Mikumo, 1996; Day *et al.*, 1998). The first model assumes that the fault could heal itself shortly after the passage of the rupture front, which allows for the rise time to remain short. The second model, however, attributes the short rise time to the heterogeneous distribution of stress drop.

To compare the rise time with rupture duration for SSEs, we focus on well-constrained events in Cascadia from Schmidt and Gao (2010). Our time-dependent GPS inversions for slip estimate the rise times on the plate interface from 1 to 2 weeks. However, temporal smoothing in the inversion likely overestimates these values. Therefore, as a proxy, the rise time used here is the average number of days required for the surface displacement to reach 95% of the maximum displacement at each GPS station. As shown in Figure 5, the event duration of SSEs is less than 3 times the rise time, whereas earthquakes have ratios significantly greater than 3. Numerical simulations of SSEs show that the fault continues to slip after the passage of the rupture front

(e.g., fig. 8 in Liu and Rice, 2009; fig. 8 in Shibazaki *et al.*, 2010; fig. 10 in Liu and Rubin, 2010), consistent with the observation of a small ratio. Our finding suggests that SSEs display less pulselike behavior than earthquakes. This may indicate that slow slip faults heal themselves more slowly after the passage of the rupture front than they do for seismogenic faults, possibly because of the slow drainage of fluids from the fault zone.

Recurrence Statistics

Recurrence models have been proposed for earthquakes, for example, the time and slip predictable model (e.g., Shimazaki and Nakata, 1980; Anagnos and Kiremidjian, 1984; Shimazaki, 2002), by assuming constant stressing rate and upper or lower stress thresholds for failure. These models provide a means to estimate the timing or size of future events, assuming that earthquakes conform to one model. For the time predictable model, the time to the next event is equal to the static stress drop released by the most recent earthquake divided by the stressing rate, which implies that a larger event requires a longer recovery time until the next one. For the slip predictable model, the fault slip released for an event is proportional to the time interval since the last event. Thus, a longer interevent period produces a larger event.

Time and slip predictable behavior is assessed by plotting the moment magnitude as a function of the recurrence interval for individual SSEs on the Cascadia subduction zone. The short and regular recurrence interval of ~14.5 months (Miller *et al.*, 2002) for SSEs in northern Cascadia makes this area ideal to test the recurrence behavior. Among the catalog of the Cascadia SSEs (Schmidt and Gao, 2010), 11 are centered near the Olympic peninsula in Washington. We calculate the recurrence interval for these events by using the time interval between the starting days of successive transient signals recorded by the GPS station ALBH (latitude 48.39° S, longitude 236.51°), which has one of the best records of SSEs in the last decade. The moment and interevent periods are plotted in Figure 6a for the slip-predictable case and in Figure 6b for the time-predictable case. Based on this limited data set, we find that the seismic moment is anticorrelated to the preevent recurrence interval for each event with a R^2 of 0.48, but has a weak positive dependence on the postevent recurrence interval with an R^2 of 0.16. This suggests that SSEs in northern Cascadia are moderately antislip predictable and weakly time predictable. Some evidence suggests a similar antislip behavior for megathrust events on subduction zones (Chile in Cisternas *et al.*, 2005; Sumatra in Sieh *et al.*, 2008; Cascadia in Goldfinger *et al.*, 2010). While few fault or SSE data sets are available to test slip predictability, this suggests that both SSEs and earthquakes may share common recurrence characteristics, at least at some locations.

The recurrence statistics presented here for an SSE sequence in northern Cascadia have some implications about the fault healing process on the SSE generation zone. We speculate that the fault is gradually healed and strengthened with time between two sequential SSEs. The stronger the fault is at the end of the inter-SSE period, the smaller the strain release for the next event, which would explain the antislip predictable behavior we see. The weak time predictability for Cascadia SSEs is consistent with the lack of evidence for time predictability for seismogenic faults (Murray and Segall, 2002; Weldon *et al.*, 2004). The significance of this recurrence behavior for SSEs is unclear. But we hope to explore this more as the catalog of events grows.

Conclusions

We explore the empirical scaling relationships of SSE source parameters that provide some insight into the underlying source process of this phenomenon. We find that the static stress drop is independent of event size, consistent with that found for earthquakes. However, the strong inverse dependence of average rupture velocity on seismic moment and the smaller ratio of duration over rise time indicate that some aspects of the underlying rupture process are different between SSEs and earthquakes. The scaling laws presented here and their comparisons with earthquakes highlight the similarities and differences of these two phenomena.

Although the implications of these SSE scaling laws are still not fully understood, the heterogeneity of fault properties appears to be important for a comprehensive interpretation of these characteristics. We find that the source zone of SSEs is consistent with an asperity model where small patches of locally high strength are distributed within a broader zone of low strength. We infer that the shear strength over the entire region is significantly less than seismogenic faults because of near-lithostatic pore pressure (Shelly *et al.*, 2006; Rubinstein *et al.*, 2007; Audet *et al.*, 2009; Nadeau and Guilhem, 2009). The low shear strength also limits the static stress drop. We propose that tremor ruptures the small asperities, whose small size results in fast rupture velocities and short rise times relative to aseismic slip. The strain on the surrounding fault is released by aseismic slip in a less pulselike mode of rupture than do earthquakes. The presence of fluids facilitates low stress drops, and the interaction of the fluids with the fault zone may delay the healing process after the passage of the rupture front but more effectively help to strengthen the fault in the long term.

Data and Resources

All data used in this study came from published sources listed in the references and in Ⓔ Table S1 (available in the electronic supplement to this paper). Slow slip events on the Cascadia subduction zone are calculated by Haiying Gao. Data for earthquakes plotted in Figure 3 are obtained from the Seismology Observatory at University of Michigan.

Acknowledgments

We thank those authors who shared their inversion results with us in an effort to explore the general scaling laws for slow slip events. We also thank Yajing Liu and Bunichiro Shibazaki for discussions of their numerical modeling and thoughtful suggestions. We thank two anonymous reviewers and the associate editor for helpful comments and reviews of the manuscript. This work was funded by the National Science Foundation (EAR-0548272) and the U.S. Geological Survey (G10AP00049).

References

Aki, K. (1979). Characterization of barriers on an earthquake fault, *J. Geophys. Res.* **84,** 6140–6148.

Anagnos, T., and A. S. Kiremidjian (1984). Stochastic time-predictable model for earthquake occurrences, *Bull. Seismol. Soc. Am.* **74,** 2593–2611.

Ando, R., R. Nakata, and T. Hori (2010). A slip pulse model with fault heterogeneity for low-frequency earthquakes and tremor along plate interfaces, *Geophys. Res. Lett.* **37,** L10310, doi: 10.1029/2010GL043056.

Ariyoshi, K., T. Hori, J.-P. Ampuero, Y. Kaneda, T. Matsuzawa, R. Hino, and A. Hasegawa (2009). Influence of interaction between small asperities on various types of slow earthquakes in a 3-D simulation for a subduction plate boundary, *Gondwana Res.* **16,** 534–544, doi: 10.1016/j.gr.2009.03.006.

Audet, P., M. G. Bostock, N. I. Christensen, and S. M. Peacock (2009). Seismic evidence for overpressured subducted oceanic crust and megathrust fault sealing, *Nature* **457,** 76–78, doi: 10.1038/nature07650.

Baumont, D., F. Courboulex, O. Scotti, N. S. Melis, and G. Stavrakakis (2002). Slip distribution of the M_w 5.9, 1999 Athens earthquake inverted from regional seismological data, *Geophys. Res. Lett.* **29,** no. 15, doi: 10.1029/2001GL014261.

Beeler, N. M., and T. E. Tullis (1996). Self-healing slip pulse in dynamic rupture models due to velocity-dependent strength, *Bull. Seismol. Soc. Am.* **86,** 1130–1148.

Beroza, G. C., and T. Mikumo (1996). Short slip duration in dynamic rupture in the presence of heterogeneous fault properties, *J. Geophys. Res.* **101,** 22,449–22,460.

Beroza, G. C., and P. Spudich (1988). Linearized inversion for fault rupture behavior: Application to the 1984 Morgan Hill, California, earthquake, *J. Geophys. Res.* **93,** 6275–6296.

Boatwright, J. (1988). The seismic radiation from composite models of faulting, *Bull. Seismol. Soc. Am.* **78,** 489–508.

Brodsky, E. E., and J. Mori (2007). Creep events slip less than ordinary earthquakes, *Geophys. Res. Lett.* **34,** L16309, doi: 10.1029/2007GL030917.

Brown, K. M., M. D. Tryon, H. R. DeShon, L. M. Dorman, and S. Y. Schwartz (2005). Correlated transient fluid pulsing and seismic tremor in the Costa Rica subduction zone, *Earth Planet. Sci. Lett.* **238,** 189–203, doi: 10.1016/j.epsl.2005.06.055.

Cisternas, M., B. F. Atwater, F. Torrejón, Y. Sawai, G. Machuca, M. Lagos, A. Eipert, C. Youlton, I. Salgado, T. Kamataki, M. Shishikura, C. P. Rajendran, J. K. Malik, Y. Rizal, and M. Husni (2005). Predecessors of the giant 1960 Chile earthquake, *Nature* **437,** 404–407, doi: 10.1038/nature03943.

Correa-Mora, F., C. DeMets, E. Cabral-Cano, B. Marquez-Azua, and O. Diaz-Molina (2008). Interplate coupling and transient slip along the subduction interface beneath Oaxaca, Mexico, *Geophys. J. Int.* doi: 10.1111/j.1365-246X.2008.03910.x.

Correa-Mora, F., C. DeMets, E. Cabral-Cano, O. Diaz-Molina, and B. Marquez-Azua (2009). Transient deformation in southern Mexico in 2006 and 2007: Evidence for distinct deep-slip patches beneath Guerrero and Oaxaca, *G³* **10,** Q02S12, doi: 10.1029/2008GC002211.

Day, S. M. (1982). Three-dimensional finite difference simulation of fault dynamics: Rectangular faults with fixed rupture velocity, *Bull. Seismol. Soc. Am.* **72,** 705–727.

Day, S. M., G. Yu, and D. J. Wald (1998). Dynamic stress changes during earthquake rupture, *Bull. Seismol. Soc. Am.* **88,** 512–522.

Douglas, A., J. Beavan, L. Wallace, and J. Townend (2005). Slow slip on the northern Hikurangi subduction interface, New Zealand, *Geophys. Res. Lett.* **32,** L16305, doi: 10.1029/2005GL023607.

Furumoto, M., and I. Nakanihshi (1983). Source times and scaling relations of large earthquakes, *J. Geophys. Res.* **88,** 2191–2198.

Geller, R. J. (1976). Scaling relations for earthquake source parameters and magnitudes, *Bull. Seismol. Soc. Am.* **66,** 1501–1523.

Goldfinger, C., C. H. Nelson, A. Morey, J. E. Johnson, J. Gutierrez-Pastor, A. T. Eriksson, E. Karabanov, J. Patton, E. Gracia, R. Enkin, A. Dallimore, G. Dunhill, and T. Vallier (2011). Turbidite event history: Methods and implications for Holocene paleoseismicity of the Cascadia subduction zone, *USGS Profess. Pap. 1661-F*, Reston, Virginia, U.S. Geological Survey, 178, in press.

Hanks, T. C., and W. H. Bakun (2002). A bilinear source-scaling model for $M - \log A$ observations of continental earthquakes, *Bull. Seismol. Soc. Am.* **92,** 1841–1846.

Hanks, T. C., and W. H. Bakun (2008). $M - \log A$ observations for recent large earthquakes, *Bull. Seismol. Soc. Am.* **98,** 490–494.

Hawthorne, J. C., and A. M. Rubin (2010). Tidal modulation of slow slip in Cascadia, *J. Geophys. Res.* **115,** B09406, doi: 10.1029/2010JB007502.

Heaton, T. H. (1990). Evidence for and implications of self-healing pulses of slip in earthquake rupture, *Phys. Earth Planet. In.* **64,** 1–20.

Hernandez, B., N. M. Shapiro, S. K. Singh, J. F. Pacheco, F. Cotton, M. Campillo, A. Iglesias, V. Cruz, J. M. Gómez, and L. Alcántara (2001). Rupture history of September 30, 1999 intraplate earthquake of Oaxaca, Mexico ($M_W = 7.5$) from inversion of strong-motion data, *Geophys. Res. Lett.* **28,** no. 2, 363–366, doi: 10.1029/2000GL011975.

Hirose, H., and K. Obara (2005). Repeating short- and long-term slow slip events with deep tremor activity around the Bungo channel region, southwest Japan, *Earth Planet. Sci. Lett.* **57,** 961–972.

Hirose, H., and K. Obara (2006). Short-term slow slip and correlated tremor episodes in the Tokai region, central Japan, *Geophys. Res. Lett.* **33,** L17311, doi: 10.1029/2006GL026579.

Hirose, H., and K. Obara (2010). Recurrence behavior of short-term slow slip and correlated nonvolcanic tremor episodes in western Shikoku, southwest Japan, *J. Geophys. Res.* **115,** B00A21, doi: 10.1029/2008JB006050.

Houston, H. (2001). Influence of depth, focal mechanism, and tectonic setting on the shape and duration of earthquake source time functions, *J. Geophys. Res.* **106,** 11,137–11,150.

Houston, H., B. G. Delbridge, A. G. Wech, and K. C. Creager (2011). Rapid tremor reversals in Cascadia generated by a weakened plate interface, *Nat. Geosci.* **4,** 404–409, doi: 10.1038/ngeo1157.

Hwang, R.-D., G.-K. Yu, and J.-H. Wang (2001). Rupture directivity and source-process time of the September 20, 1999 Chi-Chi, Taiwan, earthquake estimated from Rayleigh-wave phase velocity, *Earth Planet. Sci. Lett.* **53,** 1171–1176.

Ide, S. (2008). A Brownian walk model for slow earthquakes, *Geophys. Res. Lett.* **35,** L17301, doi: 10.1029/2008GL034821.

Ide, S. (2010). Quantifying the time function of nonvolcanic tremor based on a stochastic model, *J. Geophys. Res.* **115,** B08313, doi: 10.1029/2009JB000829.

Ide, S., G. C. Beroza, D. Shelly, and T. Uchide (2007). A scaling law for slow earthquakes, *Nature* **447,** 76–79.

Ide, S., K. Imanishi, Y. Yoshida, G. C. Beroza, and D. R. Shelly (2008). Bridging the gap between seismically and geodetically detected slow earthquakes, *Geophys. Res. Lett.* **35,** L10305, doi: 10.1029/2008GL034014.

Ishii, M., P. M. Shearer, H. Houston, and J. E. Vidale (2005). Extent, duration and speed of the 2004 Sumatra–Andaman earthquake imaged by the Hi-Net array, *Nature* **435,** 933–936, doi: 10.1038/nature03675.

Ito, Y., and K. Obara (2006). Very low frequency earthquakes within accretionary prisms are very low stress-drop earthquakes, *Geophys. Res. Lett.* **33,** L09302, doi: 10.1029/2006GL025883.

Ito, Y., K. Obara, K. Shiomi, S. Sekine, and H. Hirose (2007). Slow earthquakes coincident with episodic tremors and slow slip events, *Science* **315,** 503–506, doi: 10.1126/science.1134454.

Ji, C., D. J. Wald, and D. V. Helmberger (2002). Source description of the 1999 Hector Mine, California, earthquake, Part I: Wavelet domain inversion theory and resolution analysis, *Bull. Seismol. Soc. Am.* **92,** 1192–1207, doi: 10.1785/0120000916.

Johnson, L. R., and R. M. Nadeau (2002). Asperity model of an earthquake: Static problem, *Bull. Seismol. Soc. Am.* **92,** 672–686.

Kanamori, H., and D. L. Anderson (1975). Theoretical basis of some empirical relations in seismology, *Bull. Seismol. Soc. Am.* **65,** 1073–1095.

Kanamori, H., D. L. Anderson, and T. H. Heaton (1998). Frictional melting during the rupture of the 1994 Bolivian earthquake, *Science* **279,** 839–842.

Linde, A. T., M. T. Gladwin, M. J. S. Johnston, R. L. Gwyther, and R. G. Bilham (1996). A slow earthquake sequence on the San Andreas fault, *Nature* **383,** 65–68, doi: 10.1038/383065a0.

Liu, Y., and J. R. Rice (2009). Slow slip predictions based on granite and gabbro friction data compared to GPS measurements in northern Cascadia, *J. Geophys. Res.* **114,** B09407, doi: 10.1029/2008JB006142.

Liu, Y., and A. M. Rubin (2010). Role of fault gouge dilatancy on aseismic deformation transients, *J. Geophys. Res.* **115,** B10414, doi: 10.1029/2010JB007522.

Marone, C. J., C. H. Scholz, and R. Bilham (1991). On the mechanics of earthquake afterslip, *J. Geophys. Res.* **96,** 8441–8452.

McCausland, W. A., K. C. Creager, M. L. Rocca, and S. D. Malone (2010). Short-term and long- term tremor migration patterns of the Cascadia 2004 tremor and slow slip episode using small aperture seismic arrays, *J. Geophys. Res.* **115,** B00A24, doi: 10.1029/2008JB006063.

Meade, B. J., and J. P. Loveless (2009). Predicting the geodetic signature of $M_W \geq 8$ slow slip events, *Geophys. Res. Lett.* **36,** L01306, doi: 10.1029/2008GL036364.

Miller, M., T. Melbourne, D. J. Johnson, and W. Q. Sumner (2002). Periodic slow earthquakes from the Cascadia subduction zone, *Science* **295,** 2423.

Montgomery-Brown, E. K., P. Segall, and A. Miklius (2009). Kilauea slow slip events: Identification, source inversions, and relation to seismicity, *J. Geophys. Res.* **114,** B00A03, doi: 10.1029/2008JB006074.

Murray, J., and P. Segall (2002). Testing time-predictable earthquake recurrence by direct measurement of strain accumulation and release, *Nature* **419,** 287–291.

Nadeau, R. M., and A. Guilhem (2009). Nonvolcanic tremor evolution and the San Simeon and Parkfield, California, earthquakes, *Science* **325,** 191–193, doi: 10.1126/science.1174155.

Nakata, R., R. Ando, T. Hori, and S. Ide (2011). Generation mechanism of slow earthquakes: Numerical analysis based on a dynamic model with brittle-ductile mixed fault heterogeneity, *J. Geophys. Res.* **116,** B08308, doi: 10.1029/2010JB008188.

Obara, K. (2002). Nonvolcanic deep tremor associated with subduction in southwest Japan, *Science* **296,** 1679–1681.

Obara, K. (2010). Phenomenology of deep slow earthquake family in southwest Japan: Spatiotemporal characteristics and segmentation, *J. Geophys. Res.* **115,** B00A25, doi: 10.1029/2008JB006048.

Obara, K., H. Hirose, F. Yamamizu, and K. Kasahara (2004). Episodic slow slip events accompanied by non-volcanic tremors in southwest Japan subduction zone, *Geophys. Res. Lett.* **31,** L23602, doi: 10.1029/2004GL020848.

Peng, Z., and J. Gomberg (2010). An integrated perspective of the continuum between earthquakes and slow-slip phenomena, *Nat. Geosci.* **3,** 599–607, doi: 10.1038/ngeo940.

Rogers, G., and H. Dragert (2003). Episodic tremor and slip on the Cascadia subduction zone: The chatter of silent slip, *Science* **300,** 1942–1943, doi: 10.1126/science.1084783.

Rubin, A. M. (2011). Designer friction laws for bimodal slow slip propagation speeds, *G*^{3} **12,** Q04007, doi: 10.1029/2010GC003386.

Rubinstein, J. L., J. Vidale, J. Gomberg, P. Bodin, K. C. Creager, and S. Malone (2007). Non-volcanic tremor driven by large transient shear stresses, *Nature* **448,** 579–582, doi: 10.1038/nature06017.

Schmidt, D. A., and H. Gao (2010). Source parameters and time-dependent slip distributions of slow slip events on the Cascadia subduction zone from 1998 to 2008, *J. Geophys. Res.* **115,** B00A18, doi: 10.1029/2008JB006045.

Schwartz, S. Y., and J. M. Rokosky (2007). Slow slip events and seismic tremor at circum-Pacific subduction zones, *Rev. Geophys.* **45,** RG3004, doi: 10.1029/2006RG000208.

Segall, P., E. K. Desmarais, D. Shelly, A. Miklius, and P. Cervelli (2006). Earthquakes triggered by silent slip events on Kilauea volcano, Hawaii, *Nature* **442,** doi: 10.1038/nature04938.

Sekine, S., H. Hirose, and K. Obara (2010). Along-strike variations in short-term slow slip events in the southwest Japan subduction zone, *J. Geophys. Res.* **115,** B00A27, doi: 10.1029/2008JB006059.

Shelly, D. R., G. C. Beroza, and S. Ide (2007). Complex evolution of transient slip derived from precise tremor locations in western Shikoku, Japan, *G*^{3} **8,** Q10014, doi: 10.1029/2007GC001640.

Shelly, D. R., G. C. Beroza, H. Zhang, C. H. Thurber, and S. Ide (2006). High-resolution subduction zone seismicity and velocity structure beneath Ibaraki Prefecture, Japan, *J. Geophys. Res.* **111,** B06311, doi: 10.1029/2005JB004081.

Shibazaki, B., S. Bu, T. Matsuzawa, and H. Hirose (2010). Modeling the activity of short-term slow slip events along deep subduction interfaces beneath Shikoku, southwest Japan, *J. Geophys. Res.* **115,** B00A19, doi: 10.1029/2008JB006057.

Shimazaki, K. (2002). Long-term probabilistic forecast in Japan and time-predictable behavior of earthquake recurrence, *Seismotectonics in Convergent Plate Boundary*, Y. Fujinawa and A. Yoshida (Editors), 37–43.

Shimazaki, K., and T. Nakata (1980). Time-predictable recurrence model for large earthquakes, *Geophys. Res. Lett.* **7,** 279–282.

Sieh, K., D. H. Natawidjaja, A. J. Meltzner, C. Shen, H. Cheng, K. Li, B. W. Suwargadi, J. Galetzka, B. Philibosian, and R. L. Edwards (2008). Earthquake supercycles inferred from sea-level changes recorded in the corals of west Sumatra, *Science* **322,** 1674–1678, doi: 10.1126/science.1163589.

Wald, D. J., and T. H. Heaton (1994). Spatial and temporal distribution of slip for the 1992 Landers, California, earthquake, *Bull. Seismol. Soc. Am.* **84,** 668–691.

Wald, D. J., T. H. Heaton, and K. W. Hudnut (1996). The slip history of the 1994 Northridge, California, earthquake determined from strong ground motion, teleseismic, GPS, and leveling data, *Bull. Seismol. Soc. Am.* **86,** S49–70.

Wallace, L. M., and J. Beavan (2006). A large slow slip event on the central Hikurangi subduction interface beneath the Manawatu region, North Island, New Zealand, *Geophys. Res. Lett.* **33,** L11301, doi: 10.1029/2006GL026009.

Weldon, R., T. Fumal, and G. Biasi (2004). Wrightwood and the earthquake cycle: What a long recurrence record tells us about how faults work, *GSA Today* **14,** 4–10.

Yagi, Y. (2004). Source rupture process of the 2003 Tokachi-oki earthquake determined by joint inversion of teleseismic body wave and strong ground motion data, *Earth Planet. Sci. Lett.* **56,** 311–316.

Yagi, Y., and M. Kikuchi (2000). Source rupture process of the Kocaeli, Turkey, earthquake of August 17, 1999, obtained by joint inversion of near-field data and teleseismic data, *Geophys. Res. Lett.* **27,** no. 13, 1969–1972, doi: 10.1029/1999GL011208.

Zhang, H., R. M. Nadeau, and M. N. Toksoz (2010). Locating nonvolcanic tremors beneath the San Andreas fault using a station-pair double-difference location method, *Geophys. Res. Lett.* **37,** L13304, doi: 10.1029/2010GL043577.

Department of Geological Sciences
University of Oregon
Eugene, Oregon 97403, USA

Manuscript received 4 April 2011